




COMMUNICATION

A mutation in Ca_v2.1 linked to a severe neurodevelopmental disorder impairs channel gating

 Sidharth Tyagi¹ , Tyler R. Bendrick¹, Dilyana Filipova², Symeon Papadopoulos² , and Roger A. Bannister¹ 

Ca²⁺ flux into axon terminals via P-/Q-type Ca_v2.1 channels is the trigger for neurotransmitter vesicle release at neuromuscular junctions (NMJs) and many central synapses. Recently, an arginine to proline substitution (R1673P) in the S4 voltage-sensing helix of the fourth membrane-bound repeat of Ca_v2.1 was linked to a severe neurological disorder characterized by generalized hypotonia, ataxia, cerebellar atrophy, and global developmental delay. The R1673P mutation was proposed to cause a gain of function in Ca_v2.1 leading to neuronal Ca²⁺ toxicity based on the ability of the mutant channel to rescue the photoreceptor response in Ca_v2.1-deficient *Drosophila cacophony* larvae. Here, we show that the corresponding mutation in rat Ca_v2.1 (R1624P) causes a profound loss of channel function; voltage-clamp analysis of tsA-201 cells expressing this mutant channel revealed an ~25-mV depolarizing shift in the voltage dependence of activation. This alteration in activation implies that a significant fraction of Ca_v2.1 channels resident in presynaptic terminals are unlikely to open in response to an action potential, thereby increasing the probability of synaptic failure at both NMJs and central synapses. Indeed, the mutant channel supported only minimal Ca²⁺ flux in response to an action potential-like waveform. Application of GV-58, a compound previously shown to stabilize the open state of wild-type Ca_v2.1 channels, partially restored Ca²⁺ current by shifting mutant activation to more hyperpolarizing potentials and slowing deactivation. Consequently, GV-58 also rescued a portion of Ca²⁺ flux during action potential-like stimuli. Thus, our data raise the possibility that therapeutic agents that increase channel open probability or prolong action potential duration may be effective in combatting this and other severe neurodevelopmental disorders caused by loss-of-function mutations in Ca_v2.1.

Introduction

Ca²⁺ flux into axon terminals via P-/Q-type (Ca_v2.1) Ca²⁺ channels is the trigger for neurotransmitter vesicle release at the neuromuscular junction (NMJ) and many central synapses (Katz and Miledi, 1967; Turner et al., 1992; Uchitel et al., 1992; Dunlap et al., 1994, 1995; Wu and Saggau, 1997). Like the other two members of the Ca_v2.X subfamily, Ca_v2.1 is a heteromultimeric complex composed minimally of a principal α₁ subunit and auxiliary β and α₂δ subunits (Campiglio and Flucher, 2015). Each Ca_v2.1 α_{1A} subunit is composed of four highly conserved, membrane-bound domains (repeats I–IV) consisting of six transmembrane α-helices each (Mori et al., 1991). In addition to providing the structural elements that form the Ca²⁺-selective pore (the S5–S6 helices), each repeat contains a voltage-sensing module (the S1–S4 helices). The S4 helices are the “voltage sensors” of the channel in that they translocate extracellularly across the “gating charge transfer center” in response to depolarization, inducing conformational rearrangements that open the channel pore (Stühmer et al., 1989; Tao et al., 2010). For this

purpose, each S4 helix has evolved with five or six basic residues (positions R0–R5) lining a face of the helix that interact with acidic residues on the S2 helix to facilitate translocation (Fujita et al., 1993; Palovcak et al., 2014). Neutralization of these arginines/lysines or introduction of sterically disruptive residues can profoundly impact gating of Ca_v2.1 and other voltage-gated channels (Stühmer et al., 1989; Hans et al., 1999; Mori et al., 2000; Tottene et al., 2002; Wappl et al., 2002).

Recently, an arginine to proline substitution at the R5 position in the S4 helix of Ca_v2.1 repeat IV (R1673P) was linked to a severe disorder characterized by ataxia, generalized hypotonia, cerebellar atrophy, and global developmental delay (Luo et al., 2017). In this previous study, the R1673P mutation was found to cause a gain of function in Ca_v2.1 based on the mutant channel’s ability to rescue the photoreceptor response in 3-d-old Ca_v2.1-deficient *Drosophila cacophony* larvae. Despite the functional rescue of electroretinograms at 3 d, considerable photoreceptor neurodegeneration was observed at 30 d, leading to the idea that early

¹Department of Medicine–Cardiology Division, University of Colorado School of Medicine, Aurora, CO; ²Department of Vegetative Physiology, University of Cologne, Cologne, Germany.

Correspondence to Roger A. Bannister: roger.bannister@ucdenver.edu; Symeon Papadopoulos: symeon.papadopoulos@uk-koeln.de.

© 2019 Tyagi et al. This article is distributed under the terms of an Attribution–Noncommercial–Share Alike–No Mirror Sites license for the first six months after the publication date (see <http://www.rupress.org/terms/>). After six months it is available under a Creative Commons License (Attribution–Noncommercial–Share Alike 4.0 International license, as described at <https://creativecommons.org/licenses/by-nc-sa/4.0/>).

aberrant Ca²⁺ flux via the mutant Ca_v2.1 gives rise to chronic neuronal Ca²⁺ toxicity in *Drosophila* and, by extrapolation, humans.

Since the R1673P substitution occurs at a highly conserved position that is likely to be critical for sensing membrane potential, we were intrigued by its effect on channel gating. To determine the impact of the mutation on Ca_v2.1 function, we expressed the rat orthologue (R1624P) in a null-background cell line (tsA-201 cells) and recorded Ca²⁺ and Ba²⁺ currents using whole-cell voltage clamp (Hamill et al., 1981). Our results indicate that the R1624P mutation causes a profound loss of channel function by shifting the voltage dependence of channel activation ~25 mV to more depolarizing potentials. The alteration in channel activation implies that a significant fraction of Ca_v2.1 channels resident in presynaptic terminals remain closed during an action potential, thereby increasing the likelihood of synaptic failure at both NMJs and central synapses.

Materials and methods

Ethical approval

No animals or human subjects were used in this study.

Molecular biology

Venus-fused rat Ca_v2.1 R1624P was derived from the plasmid V-Ca_v2.1 (accession no. NM_012918), a generous gift from Dr. P.J. Kammermeier (University of Rochester School of Medicine and Dentistry, Rochester, NY; Beqollari and Kammermeier, 2013). A single G to C point mutation at bp 4,871 of V-Ca_v2.1 was introduced via the Q5 Site-Directed Mutagenesis kit (New England Biolabs) using the forward primer 5'-AAACTCCTCCC CAGGGTTACAC-3' and the reverse primer 5'-GATGAGTCGGGC AGCACG-3'. The presence of the mutation was verified by sequencing.

Cell culture and transfection

Mycoplasma-free tsA-201 cells (Sigma-Aldrich) were cultured and transfected using Lipofectamine 2000 (Thermo Fisher Scientific) as described previously (Beqollari et al., 2015). The transfection mixture contained expression plasmids encoding V-Ca_v2.1 or V-Ca_v2.1 R1624P with rat β₄ and rabbit α₂δ-1 auxiliary subunits (1 μg of each cDNA per well). The day after transfection, cells were trypsinized and replated onto 35-mm Primaria-treated plastic culture dishes (BD Falcon). Successfully transfected cells were used in experiments ~24 h later.

Confocal imaging

Images of live tsA-201 cells expressing either V-Ca_v2.1 or V-Ca_v2.1 R1624P were acquired using the confocal laser scanning microscope LSM780 (Zeiss) as described previously (Beqollari et al., 2018). Briefly, Venus was excited with the 488-nm line of an argon laser directed to the cell via a 488-nm/543-nm dual dichroic mirror. The emitted Venus fluorescence was directed to a photomultiplier equipped with a 500- to 550-nm band-pass filter.

Whole-cell electrophysiology

All electrophysiological experiments were performed at room temperature. Borosilicate pipettes (3.0–4.5 MΩ) were filled with

an internal solution containing (in mM): 140 Cs-aspartate, 10 Cs₂-EGTA, 5 MgCl₂, and 10 HEPES, pH 7.4 with CsOH. The external solution contained (in mM): 145 tetraethylammonium-Cl, 4 KCl, 2 CaCl₂ or 2 BaCl₂, 2 MgCl₂, 10 HEPES, 10 glucose, and 1 4-aminopyridine, pH 7.4 with tetraethylammonium-OH. GV-58 (Alamone) was dissolved in 100% DMSO to make a 50-mM solution and then diluted in the external recording solution just before experiments. During experiments, the GV-58 working solutions were applied through a manually operated, gravity-driven global perfusion system. Electronic compensation was used to reduce the effective series resistance. Linear components of leak and capacitive currents were corrected with -P/4 online subtraction protocols. Except where noted, filtering was at 5 kHz and digitization was at 10 kHz. Cell capacitance (C_m) was determined by integration of a transient from -80 mV to -70 mV using Clampex 9.2 (Molecular Devices) and was used to normalize current amplitudes (pA/pF). The average value of C_m was 30 ± 1 pF (n = 156 cells) and the time constant for decay of the whole-cell capacity transient (τ_m) was reduced as much as possible using the analogue compensation circuit of the amplifier; the average values of τ_m and R_a were 277 ± 8 μs and 9.3 ± 0.4 MΩ, respectively.

Peak and normalized I-V curves were fitted according to:

$$I = G_{\max}(V - V_{\text{rev}})/(1 + \exp[(V_{1/2} - V)/k_G]), \quad (1)$$

where I is the peak or normalized current for the test potential V, V_{rev} is the reversal potential, G_{max} is the maximum channel conductance, V_{1/2} is the half-maximal activation potential, and k_G is the slope factor. Tail current amplitudes (I_{tail}) were measured immediately following the onset of the repolarization from the test pulse to -40 mV. G-V relationships were obtained from the I_{tail}-V data, where individual tail current amplitudes evoked from a given test potential were normalized by the tail current amplitude produced by repolarization from +90 mV to -40 mV. Normalized I_{tail} values were subsequently fit with the equation:

$$G/G_{\max} = 1/(1 + \exp[-(V_{1/2\text{act}} - V)/k]), \quad (2)$$

where G is the tail current amplitude evoked by repolarization from a given test potential back to -40 mV, G_{max} is the normalized conductance for repolarization from +90 mV to -40 mV, V_{1/2act} is the half-maximal activation potential, and k is the slope factor. Activation kinetics were fit with a single exponential function:

$$I(t) = I_0[\exp(-t/\tau_{\text{act}})]. \quad (3)$$

To assess the rate of inactivation, current decay kinetics were expressed as half-time of total current decay during a 500-ms test step (t_{1/2decay}). Deactivation kinetics were fit with a single exponential function:

$$I_{\text{tail}}(t) = I_{\text{tail}0}[\exp(-t/\tau_{\text{deact}})]. \quad (4)$$

Ramp waveforms intended to mimic neuronal action potentials were generated using a protocol similar to that used by Bahamonde et al. (2015). Cells were depolarized by a 1-ms ramp from -80 mV to +30 mV immediately followed by a 1-ms repolarization ramp to -80 mV. For this subset of experiments, filtering was at 10 kHz and digitization was at 33 kHz. Peak currents have been expressed in pA/pF, whereas charge flux

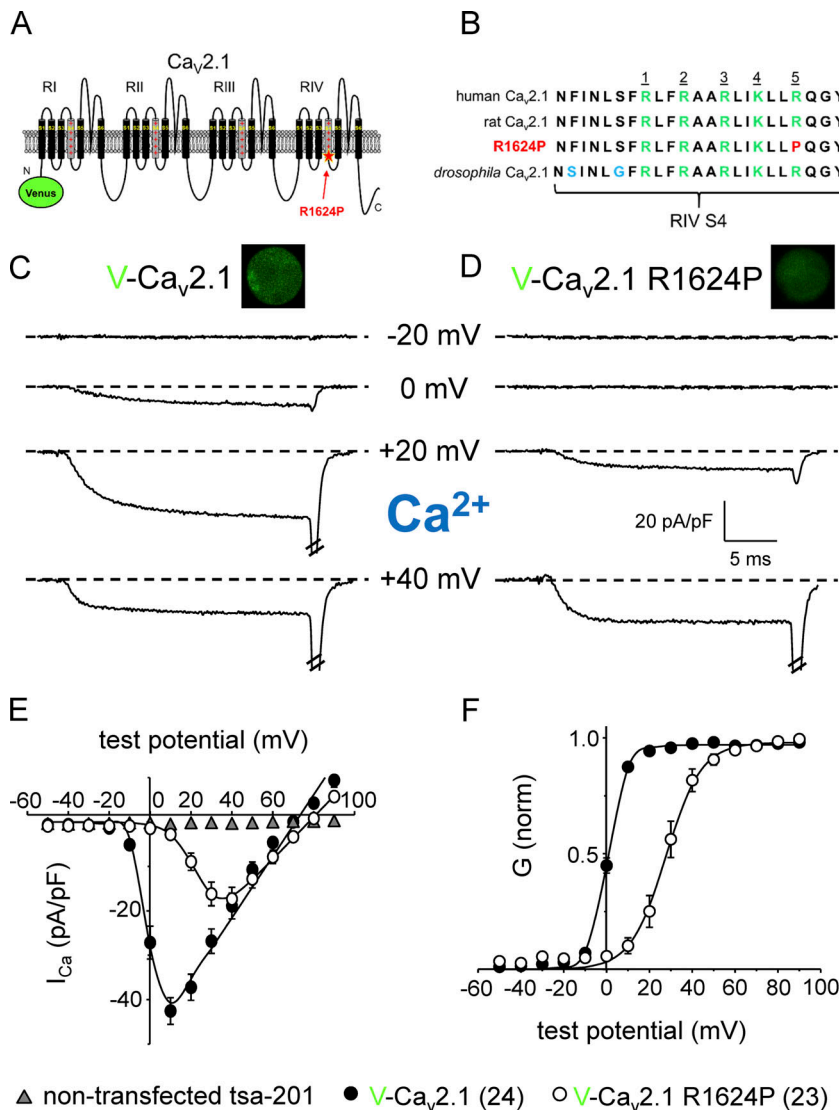


Figure 1. The R1624P mutation causes a profound depolarizing shift in Ca_v2.1 activation. (A) Schematic representation of Ca_v2.1 with Venus fluorescent protein fused to the N terminus (V-Ca_v2.1). The R to P substitution at human residue 1,673 (rat residue 1,624) is indicated by the star. (B) Sequence comparison of the RIV S4 helices of human Ca_v2.1 (GenBank accession no. NM_000068) and rat Ca_v2.1 (GenBank accession no. NM_012918), rat Ca_v2.1 with the R to P substitution at the R5 position and *Drosophila* Ca_v2.1 (UniProtKB accession no. P91645). Basic residues in positions R0–R5 are shown in green (Ca_v2.1 RIV S4 lacks a basic residue in the nominal R0 position). Nonconserved residues are in blue. (C and D) Ca²⁺ current families recorded from tsA-201 cells expressing V-Ca_v2.1 (C) or V-Ca_v2.1 R1624P (D) with β₄ and α₂δ-1. Currents were elicited by 25-ms step depolarizations from –90 mV to the indicated test potentials; the repolarization voltage was –40 mV. (E) Comparison of V-Ca_v2.1 (●; n = 24) and V-Ca_v2.1 R1624P (○; n = 23) average peak I–V relationships. Currents were evoked at 0.1 Hz by test potentials ranging from –50 mV through +90 mV in 10-mV increments. Amplitudes were normalized by capacitance (pA/pF). I–V curves are plotted according to Eq. 1 with the following respective parameters for V-Ca_v2.1 and V-Ca_v2.1 R1624P: G_{max} = 690 ± 30 and 560 ± 70 pS/pF, V_{1/2} = –0.9 ± 1.0 and 18.2 ± 1.6 mV, V_{rev} = 71.1 ± 2.6 and 77.7 ± 2.0 mV and k = 3.4 ± 0.8 and 6.2 ± 0.9 mV. (F) Normalized G–V relationships were fit with Eq. 2 with the following respective parameters for V-Ca_v2.1 and V-Ca_v2.1 R1624P: V_{1/2} = 2.3 ± 1.2 and 27.8 ± 2.1 mV; k = 4.3 ± 0.8 and 8.2 ± 1.2 mV. Error bars represent ±SEM.

was calculated as the integral of the area under the current evoked by the ramp protocol.

Statistics

Figures were made using SigmaPlot software (version 12.0; Systat Software). All data are presented as mean ± SEM. All statistical comparisons were by unpaired, two-tailed *t* test, unless otherwise noted. *P* < 0.05 was considered significant.

Online supplemental material

Figs. S1 and 2 show the R1624P substitution did not appear to affect Ca_v2.1 inactivation after 100-Hz trains or 5-s step depolarizations, respectively.

Results

The R1624P mutation causes a profound depolarizing shift in Ca_v2.1 activation

The R1673P mutation resides in the “R5” position in the voltage-sensing S4 α-helix of repeat IV of Ca_v2.1 (Mori et al., 1991; Fig. 1 A).

The repeat IV S4 helix is highly conserved from *Drosophila* to mammals (Luo et al., 2017; Fig. 1 B). For experiments, Venus fluorescent protein was fused to the N termini of wild-type rat Ca_v2.1 and to Ca_v2.1 carrying the rat equivalent of the human R1673P mutation (V-Ca_v2.1 and V-Ca_v2.1 R1624P, respectively; Fig. 1 B); the addition of a single fluorescent protein tag does not affect channel gating (Grabner et al., 1998). These constructs were expressed in tsA-201 cells with α₂δ-1 and β₄ auxiliary channel subunits (Fig. 1, C and D, insets), because these subunits promote membrane expression of the α_{1A} subunit in this heterologous system (Meza and Adams, 1998). In particular, we chose the β₄ isoform because of its overlapping expression with Ca_v2.1 at NMJs (Pagani et al., 2004; Molina-Campos et al., 2015) and in multiple cell types within the cerebellum (Volsen et al., 1997).

The whole-cell patch-clamp technique was employed to test directly whether the Ca_v2.1 R1624P mutation affects channel gating (Hamill et al., 1981). With 2 mM Ca²⁺ serving as the charge carrier, cells expressing V-Ca_v2.1 produced robust Ca²⁺ currents that peaked around +10 mV (Fig. 1, C and E). Cells expressing

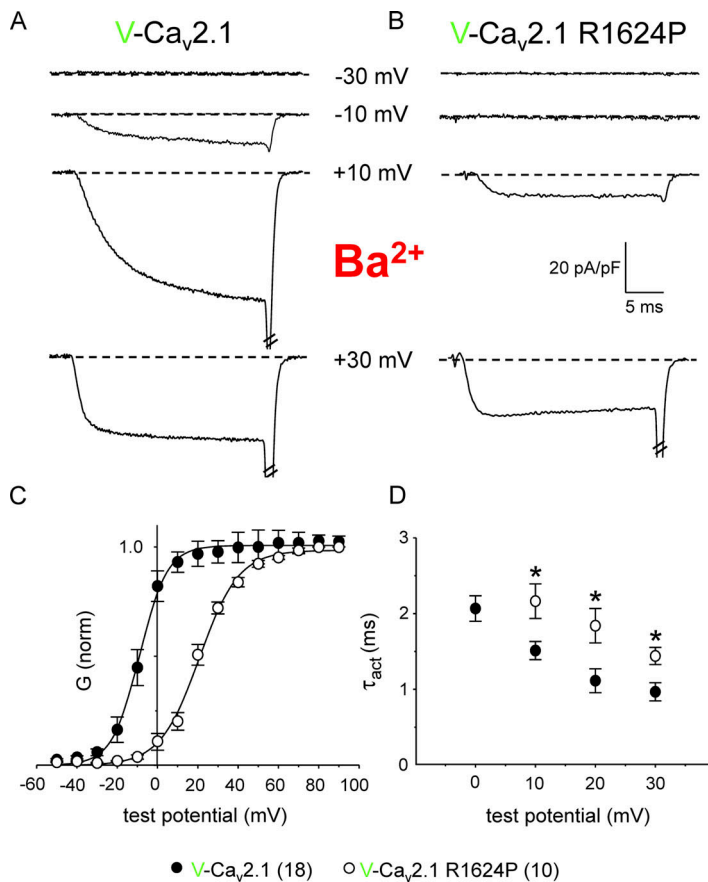


Figure 2. The R1624P mutation causes a profound depolarizing shift in the activation of Ba²⁺ currents. (A and B) Ba²⁺ current families recorded from tsA-201 cells expressing V-Ca_v2.1 (A) or V-Ca_v2.1 R1624P (B) with β₄ and α₂δ-1. Currents were elicited by 25-ms-step depolarizations from -90 mV to the indicated potentials; the repolarization voltage was -40 mV. (C) Normalized G-V relationships were fit with Eq. 2 with the following respective parameters for V-Ca_v2.1 (●; n = 16) and V-Ca_v2.1 R1624P (○; n = 10): V_{1/2} = -8.9 ± 2.3 and 20.8 ± 2.7 mV; k = 6.9 ± 0.7 and 9.7 ± 0.4 mV. (D) Comparison of activation kinetics from tsA-201 cells expressing either V-Ca_v2.1 (●; n = 16) or V-Ca_v2.1 R1624P (○; n = 10). For both channels, the activation phase was fit by Eq. 3. Only test potentials in which a substantial amount of current was present (i.e., ranging from 0 to 30 mV for V-Ca_v2.1 and 10 to 30 mV for V-Ca_v2.1 R1624P). Significant differences by two-tailed, unpaired t test are indicated (*, P < 0.05). Error bars represent ± SEM.

V-Ca_v2.1 R1624P also supported Ca²⁺ currents, but the current only developed at more depolarizing test potentials and peaked near +35 mV (Fig. 1, D and E). This marked depolarizing shift in activation of V-Ca_v2.1 R1624P relative to V-Ca_v2.1 was evident in the I-V relationship (V_{1/2} = 18.2 ± 1.6 mV, n = 23 vs. -0.89 ± 1.02 mV, n = 24, respectively; P < 0.0001; Fig. 1 E). Importantly, G_{max} values derived from the I-V relationships for V-Ca_v2.1 and V-Ca_v2.1 R1624P (690 pS/pF ± 30 and 560 ± 70 pS/pF, respectively; P > 0.05) were not significantly different, indicating that the reduction in peak current was a result of the shift rather than a substantial reduction in channel expression.

It is important to note that the V_{1/2} values obtained from the I-V relationships were influenced by an outward Cs⁺ conductance at more depolarizing potentials. To avoid any ambiguity regarding the magnitude of the shift in activation, we obtained G-V relationships from the tail currents of the same recordings. The profound depolarizing shift in activation of V-Ca_v2.1 R1624P relative to V-Ca_v2.1 persisted in the G-V relationships (V_{1/2} = 27.8 ± 2.1 mV vs. 4.3 ± 1.2 mV, respectively; P < 0.001; Fig. 1 F). Similarly, a >20-mV depolarizing shift was also observed in the G-V relationship when 2 mM Ba²⁺ was used as the charge carrier (V_{1/2} = 20.8 ± 2.7 and -8.93 ± 2.3 mV, respectively; P < 0.001; Fig. 2, A-C). Ba²⁺ current activation kinetics were fit over a range of test potentials (0–30 mV) with a single exponential function. At each test potential examined, the activation kinetics were significantly slower for tsA-201 cells expressing the mutant Ca_v2.1 construct than for those expressing the wild-type channel (P < 0.05 for all sets; Fig. 2 D).

However, the slower activation appeared to be a direct consequence of the ~25-mV shift in the voltage dependence of activation.

Deactivation is little affected by the R1624P substitution

Llinás et al. (1981) demonstrated that most of the Ca²⁺ influx at NMJs occurs during the falling phase of the action potential. Thus, alterations in Ca_v2.1 deactivation could have more profound effects on action potential-induced Ca²⁺ influx beyond those predicted merely by a shift in activation. For this reason, we assessed deactivation kinetics evoked by repolarization from peak activation (i.e., +10 mV and +30 mV for V-Ca_v2.1 and V-Ca_v2.1 R1624P, respectively) to a range of less depolarizing test potentials (Fig. 3 A). The results of these experiments showed that the wild-type channel deactivates at voltages ~20 mV more hyperpolarized relative to V-Ca_v2.1 R1624P (Fig. 3, B-D). However, the shift is largely negated when one considers the 20-mV difference in the prior depolarization, as shown in the lower traces in Fig. 3, B and C. That is, a similar magnitude of repolarization from peak activation is required for wild-type and mutant channel closure.

Inactivation kinetics are accelerated by the R1624P mutation

Timothy syndrome, another profound developmental disorder, is precipitated by a gain-of-channel-function mutation in Ca_v1.2 that retards voltage-dependent inactivation (Splawski et al., 2004, 2005). To explore the possibility of whether the R1624P mutation also causes a gain of Ca_v2.1 channel function by

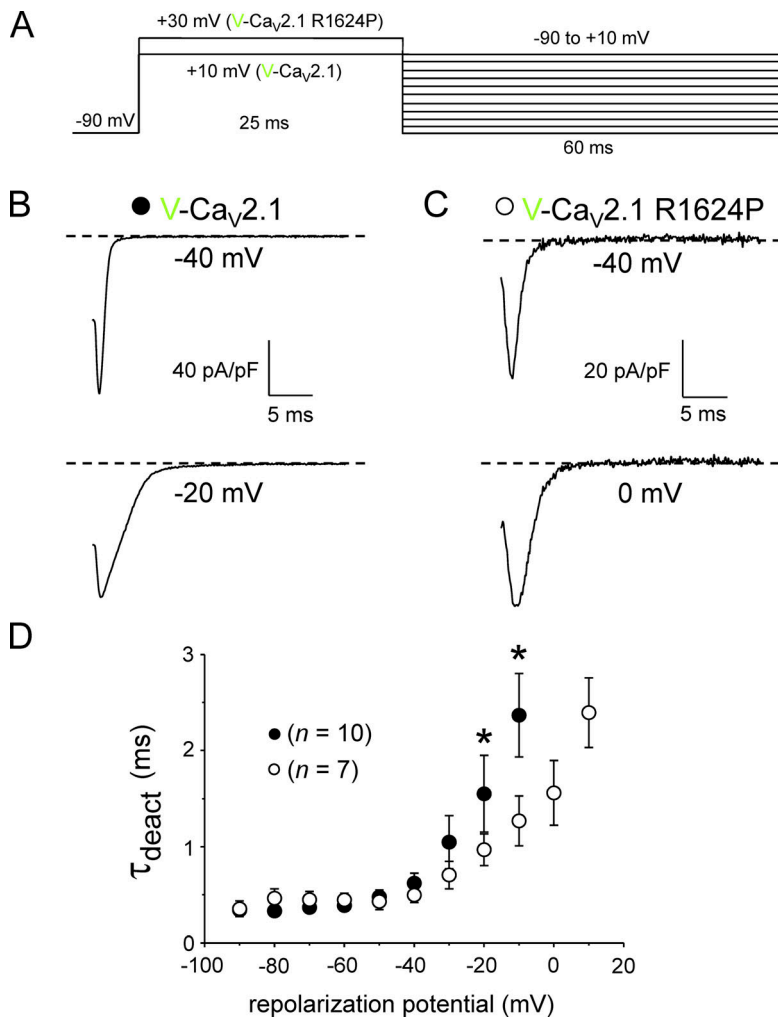


Figure 3. V-Ca_v2.1 R1624P deactivation kinetics. (A) Ba²⁺ tail currents were elicited by 60-ms repolarizations to test potentials ranging from -90 mV to +10 mV following a 25-ms depolarization from -90 mV to either +30 mV or +10 mV. (B and C) Representative Ba²⁺ tail currents recorded from tsA-201 cells expressing V-Ca_v2.1 (B) or V-Ca_v2.1 R1624P (C) following depolarization from either +10 mV for V-Ca_v2.1 or +30 mV for V-Ca_v2.1 R1624P to the indicated test potentials. (D) Comparison of deactivation kinetics from tsA-201 cells expressing either V-Ca_v2.1 (●; n = 10) or V-Ca_v2.1 R1624P (○; n = 7). For both channels, deactivation was fit by Eq. 4. Significant differences by two-tailed, unpaired t test are indicated (*, P < 0.05).

slowing voltage-dependent inactivation, we measured Ba²⁺ current decay kinetics during 500-ms depolarizations near the peak of the I-V relationships of V-Ca_v2.1 (+10 mV; Fig. 4 A) and V-Ca_v2.1 R1624P (+30 mV; Fig. 4 B). In these experiments, we found the rate of inactivation to be significantly faster for V-Ca_v2.1 R1624P relative to V-Ca_v2.1 ($t_{1/2\text{decay}} = 110 \pm 14$ ms, n = 13 vs. 270 ± 39 ms, n = 10, respectively; P < 0.001; Fig. 4 C). This difference in the rate of open-state inactivation between V-Ca_v2.1 and V-Ca_v2.1 R1624P is probably underestimated, as the wild-type current does not decay entirely during the 500-ms test potential.

While the R1624P mutation destabilizes the open state by accelerating the transition to the inactivated state, this process occurs over a time frame unlikely to have great implications for neurotransmitter release. Indeed, when inactivation was measured following a 200-ms, 100-Hz high-frequency stimulus train, there was no appreciable difference in the amount of decay of the peak current between V-Ca_v2.1 and V-Ca_v2.1 R1624P (P₂/P₁ = 0.958 ± 0.007 , n = 10 vs. 0.946 ± 0.006 , n = 10, respectively; P > 0.05; Fig. S1). There was also no difference in inactivation from the closed state between V-Ca_v2.1 and V-Ca_v2.1 R1624P ($V_{1/2\text{inact}} = -33.3 \pm 2.2$ mV, n = 13 vs. -29.1 ± 3.4 mV, n = 8, respectively; P > 0.05; Fig. S2).

The Roscovitine derivative GV-58 promotes Ca²⁺ flux via both Ca_v2.1 and Ca_v2.1 R1624P

Since the cyclin-dependent kinase inhibitor Roscovitine increases neurotransmitter release at NMJs and central synapses by promoting Ca²⁺ flux via P-/Q-type channels (Yan et al., 2002; Wen et al., 2013), we tested the effects of its higher-affinity derivative GV-58 (Tarr et al., 2013; Wu et al., 2018) on currents mediated by V-Ca_v2.1 and V-Ca_v2.1 R1624P. In these experiments, GV-58 (12.5 μM) expectedly slowed deactivation of V-Ca_v2.1 ($\tau_{\text{deact}} = 0.69 \pm 0.07$ ms vs. 5.79 ± 0.48 ms before and during GV-58 application, respectively; P < 0.001; paired t test; Fig. 5, A and C). GV-58 also augmented step current by shifting V-Ca_v2.1 activation to slightly more hyperpolarizing potentials (1.7 ± 1.3 mV vs. -5.7 ± 2.8 mV before and during drug application, respectively; P < 0.001, paired t test; n = 8, Fig. 5, B and D). Similar effects on deactivation were observed when GV-58 was applied to tsA-201 cells expressing V-Ca_v2.1 R1624P ($\tau_{\text{deact}} = 1.02 \pm 0.03$ ms vs. 4.41 ± 0.45 ms before and during GV-58 application, respectively; P < 0.001; paired t test; Fig. 5, E and G). However, the hyperpolarizing shift in activation induced by GV-58 was approximately three times larger for V-Ca_v2.1 R1624P than the shift observed with V-Ca_v2.1 (27.9 ± 2.2 mV vs. 10.8 ± 1.9 mV before and during drug application, respectively; P <

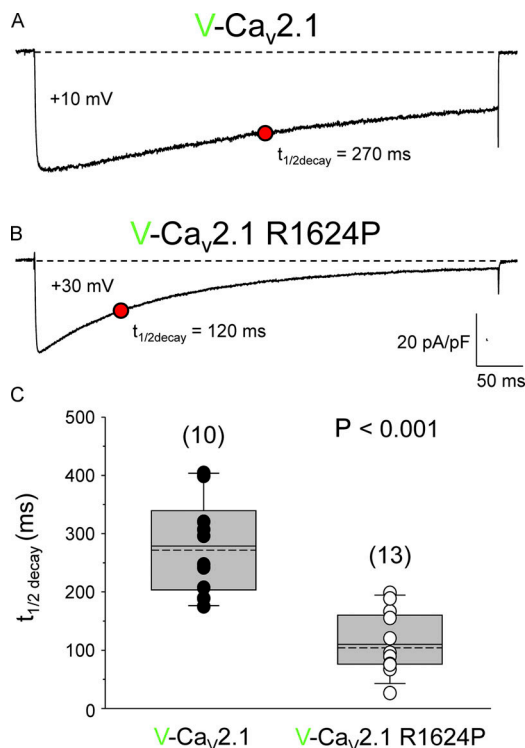


Figure 4. Open-state inactivation of $\text{Ca}_V2.1$ is accelerated by the R1624P mutation. (A and B) Representative Ba^{2+} currents recorded from tsA-201 cells expressing V- $\text{Ca}_V2.1$ (A) or V- $\text{Ca}_V2.1$ R1624P (B) near the peak of the I-V relationship for either channel. Currents were elicited by 500-ms depolarizations from -90 mV to $+10$ mV (A) and $+30$ mV (B). In both A and B, half-times of decay are indicated by the red dot. (C) Summary of half-times of current decay for V- $\text{Ca}_V2.1$ (●; $n = 10$) and V- $\text{Ca}_V2.1$ R1624P (○; $n = 13$). Means and medians are indicated by the dashed and solid black lines of the boxes, respectively. Boxes represent the 25th/75th percentiles. Bars represent the 5th/95th percentiles. A significant difference by two-tailed, unpaired t test is indicated ($P < 0.001$).

0.001 , paired t test; $n = 7$, Fig. 5, F and H). The consequence of this shift was that significantly more Ca^{2+} current mediated by V- $\text{Ca}_V2.1$ R1624P could be evoked by step depolarizations in the range of maximal activation of the wild-type channel (Fig. 5, E, F, and H).

GV-58 increases Ca^{2+} flux via both V- $\text{Ca}_V2.1$ and V- $\text{Ca}_V2.1$ R1624P in response to an action potential-like waveform

The ~ 25 -mV depolarizing shift in activation for V- $\text{Ca}_V2.1$ R1624P relative to V- $\text{Ca}_V2.1$ suggests that the mutant channel will only be minimally activated by an action potential. To investigate this idea more rigorously, we evoked Ca^{2+} flux via an action potential-like voltage-clamp protocol similar to that used by Bahamonde et al. (2015) to assess flux via heterologously expressed $\text{Ca}_V2.1$ channels. Briefly, this stimulus consisted of a 1.0-ms rising phase from -80 mV to $+30$ mV followed by a 1.0-ms decline back to -80 mV (Fig. 6, A and D, top panels). Robust Ca^{2+} influx via V- $\text{Ca}_V2.1$ was observed using this protocol (Fig. 6 A). Specifically, the evoked current reached -4.4 ± 0.7 pA/pF in amplitude ($n = 8$; Fig. 6 B), and the total charge flux was -2.7 ± 0.3 nC/ μF (Fig. 6 C). By contrast, V- $\text{Ca}_V2.1$ R1624P exhibited little current, as assessed via amplitude (-1.4 ± 0.2 pA/pF, $n = 7$; $P <$

0.001 vs. that for V- $\text{Ca}_V2.1$) and flux (-0.7 ± 0.2 nC/ μF ; $P < 0.001$ vs. that for V- $\text{Ca}_V2.1$), supporting the idea that the human orthologue of V- $\text{Ca}_V2.1$ R1624P supports little or no Ca^{2+} influx at presynaptic terminals in response to depolarizations in the physiological range (Fig. 6, D-F).

Since GV-58 increases channel P_o by (1) shifting the voltage dependence of activation to less depolarizing potentials (Fig. 5, D and H) and (2) slowing deactivation (Tarr et al., 2013; Wu et al., 2018; Fig. 5, A-C and G), we investigated whether GV-58 could enhance Ca^{2+} flux via V- $\text{Ca}_V2.1$ and V- $\text{Ca}_V2.1$ R1624P in response to action potential-like stimuli. In regard to V- $\text{Ca}_V2.1$, GV-58 greatly enhanced both current amplitude by $272.5 \pm 33.3\%$ and charge flux by $282.6 \pm 29.0\%$ ($n = 8$; both $P < 0.001$; Fig. 6, A-C). Current amplitude and charge flux were both increased by GV-58 in cells expressing V- $\text{Ca}_V2.1$ R1624P ($315.6 \pm 59.8\%$ and $288.5 \pm 34.7\%$, respectively, $n = 7$; both $P < 0.001$; Fig. 6, D-F), though the drug failed to fully rescue channel function.

Discussion

Our results show that the R1624P substitution caused an ~ 25 -mV depolarizing shift in $\text{Ca}_V2.1$ activation (Figs. 1 and 2) without great effect on channel activation kinetics (Fig. 2 D) or deactivation (Fig. 3). The R1624P mutation accelerated inactivation from the open state during 500-ms step depolarizations (Fig. 4), but did not appear to affect inactivation following a 100-Hz train (Fig. S1) or individual 5-s depolarizations (Fig. S2). The primary implication of these data are that action potentials are likely insufficient to gate a significant portion of $\text{Ca}_V2.1$ R1624P channels. Since Ca^{2+} flux into axon terminals via $\text{Ca}_V2.1$ is the trigger for neuromuscular communication (Katz and Miledi, 1967; Turner et al., 1992; Dunlap et al., 1994, 1995; Wu and Saggau, 1997), the ~ 25 -mV depolarizing shift in activation of the rat $\text{Ca}_V2.1$ mutant suggests that more frequent synaptic failure at the NMJ contributes to the hypotonia and muscle weakness associated with human $\text{Ca}_V2.1$ R1673P. Likewise, the ataxia, cerebellar atrophy and developmental delay may potentially be attributed to synaptic failures within the cerebellum and other regions of the central nervous system where $\text{Ca}_V2.1$ is expressed. Our data indicating that Ca^{2+} flux via $\text{Ca}_V2.1$ R1624P is reduced in response to an action potential-like stimulus provide support for this idea (Fig. 6).

The finding that the R1624P mutation profoundly impairs channel voltage-sensitivity contrasts, at least superficially, with the observations of an earlier study in which the photoreceptor response was rescued by the $\text{Ca}_V2.1$ R1673P mutant in 3-d-old *cacophony* ($\text{Ca}_V2.1$ -deficient) *Drosophila* larvae (Luo et al., 2017). Multiple explanations could account for the seemingly diametric effects of the two approaches, including elevated expression levels of the mutant or compensation from other *Drosophila* Ca^{2+} channel isoforms during early larval development. Moreover, it is unknown whether the R to P substitution at the R5 position in the *cacophony* channel causes a similar impediment of gating to the corresponding mutation in the rat $\text{Ca}_V2.1$ channel. Needless to say, further investigation is required to determine how a loss of function on the molecular level translates to a toxic gain of function on the organismal level in flies.

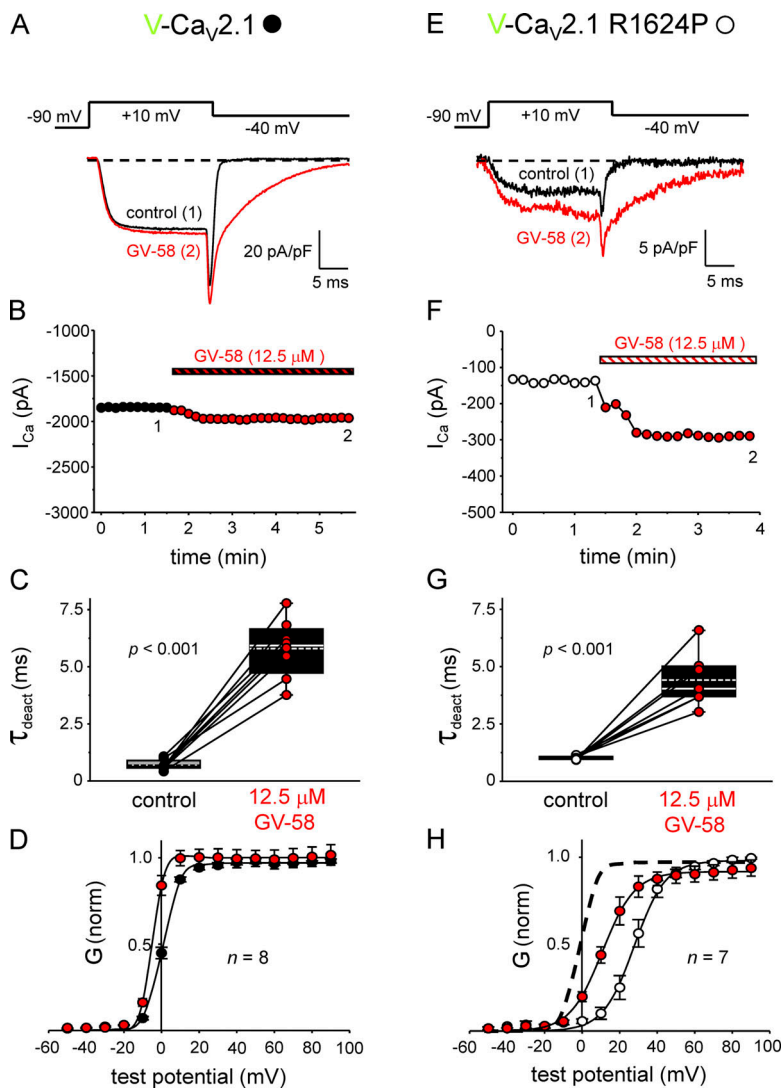


Figure 5. GV-58 promotes Ca²⁺ flux via both Ca_v2.1 and Ca_v2.1 R1624P. (A) Ca²⁺ currents recorded before (1) and during (2) application of 12.5 μM GV-58 to a tsA-201 cell expressing V-Ca_v2.1, β₄, and α₂δ-1. (B) Time course of step current amplitude before (black filled circles) and during (red filled circles) GV-58 application. Currents were evoked by the protocol illustrated in A at 0.1 Hz. Numbers correspond to traces shown in A. (C) Comparison of τ_{deact} of V-Ca_v2.1 tail currents evoked by repolarization from +10 mV to -40 mV in the absence (black filled circles) or presence (red filled circles) of GV-58 (n = 8). (D) Normalized G-V relationships before and during application of GV-58. Currents were evoked at 0.1 Hz by test potentials ranging from -50 mV to +90 mV in 10-mV increments. G-V curves are plotted according to Eq. 2 with the respective parameters for control and GV-58: V_{1/2} = 1.7 ± 1.3 and -5.7 ± 2.8 mV and k = 4.8 ± 0.4 and 5.6 ± 0.8 mV. (E) Ca²⁺ currents recorded before (1) and during (2) application of 12.5 μM GV-58 to a tsA-201 cell expressing V-Ca_v2.1 R1624P, β₄, and α₂δ-1. (F) The corresponding time course. (G) Comparison of V-Ca_v2.1 R1624P deactivation upon repolarization from +10 mV to -40 mV in the absence (open circles) or presence (red circles) of GV-58 (n = 7). (H) Normalized G-V relationships for V-Ca_v2.1 R1624P before and during application of GV-58. The respective G-V fit parameters for control and GV-58 were V_{1/2} = 27.9 ± 2.2 and 10.8 ± 1.9 mV and k = 8.3 ± 0.4 and 8.6 ± 0.5 mV. For reference, the G-V curve for wild-type V-Ca_v2.1 in the absence of GV-58 is shown as a dashed black line. As in Figure 3, tail currents were fit by Eq. 4. Means and medians in C and G are indicated by the dashed and solid lines of the boxes, respectively. Boxes represent the 25th/75th percentiles. Bars represent the 5th/95th percentiles. In D and H, error bars represent ±SEM. Significant differences by two-tailed, paired t test are indicated.

While the nameless disorder described by Luo et al. (2017) shares a genetic basis and some overlapping characteristics with episodic ataxia type 2 and spinocerebellar ataxia type 6 (Piétrobon, 2010), it is representative of a distinct and growing family of more severe developmental disorders that are beginning to be revealed more frequently with whole-exome sequencing techniques (Blumkin et al., 2010; Romaniello et al., 2010; Lv et al., 2017; Travaglini et al., 2017). Perhaps the most relevant example is a proline to leucine substitution at residue 1,353, which resides in the S4 helix of repeat III (Weyhrauch et al., 2016). This particular mutation, which essentially ablated the ability of Ca_v2.1 to support Ca²⁺ currents in tsA-201 cells, resulted in a similar syndrome to the one precipitated by the R1673P mutation; both disorders are characterized not only by ataxia but also include hypotonia, language deficits, and global developmental delay. Even though P1353L and R1673P both cause loss of channel function, the mechanisms by which they do so seem to differ. The former mutation appears to prevent expression/trafficking of the channel, while the latter makes the channel far less sensitive to elevations in membrane potential. Thus, the pathology of P1353L is likely to be a

consequence of haploinsufficiency (Weyhrauch et al., 2016). By contrast, the ability of the rat equivalent of R1673P to form functional channels that are efficiently trafficked to the membrane in our expression system suggests that the mutant channel exerts a dominant-negative effect in vivo by competing with wild-type Ca_v2.1 for tightly regulated “slots” at presynaptic terminals (Cao et al., 2004; Cao and Tsien, 2010). In this regard, the impaired gating of the mutant channel likely diminishes synaptic vesicle release probability, as the density of functional Ca_v2.1 channels has been found recently to correlate tightly with synaptic strength at the calyx of Held synapse in mice (Lübbert et al., 2019).

Impairment of Ca_v2.1 function has been reported to weaken neuromuscular transmission in both episodic ataxia type 2 patients and the *leaner* mouse model of the disease (Jen et al., 2001; Maselli et al., 2003; Kaja et al., 2008; Piétrobon, 2010). Similarly, a zebrafish mutant with a spontaneous tyrosine to asparagine mutation occurring at position 1,662 of the Ca_v2.1b isoform was shown to have greatly impaired mechanically induced escape responses. The motility impairment was ascribed to the diminished frequency and amplitudes of end-plate currents

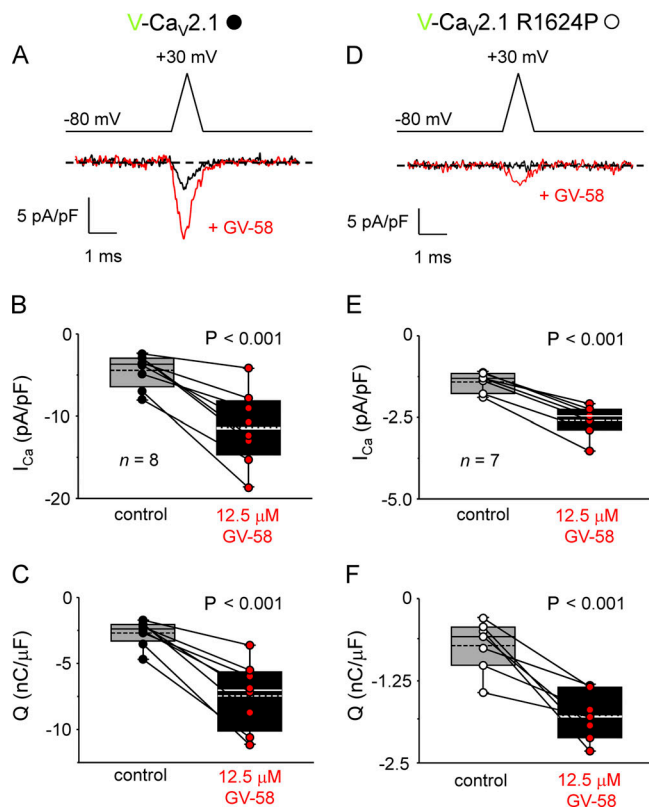


Figure 6. GV-58 increases Ca^{2+} flux via V-Ca $_v$ 2.1 and V-Ca $_v$ 2.1 R1624P in response to an action potential-like waveform. (A and D) Ca^{2+} currents recorded before (1) and during (2) application of 12.5 μM GV-58 to tsA-201 cells expressing either V-Ca $_v$ 2.1 (A) or V-Ca $_v$ 2.1 R1624P (D). In both cases, Ca^{2+} currents were evoked by an action potential-like waveform similar to that used by Bahamonde et al. (2015). Specifically, this stimulus consisted of a 1-ms rising phase from -80 mV to $+30$ mV followed by a 1-ms decline back to -80 mV (illustrated in A and D, top). (B and C) Comparison of current amplitudes (B) and total charge flux (C) for cells expressing V-Ca $_v$ 2.1 in the absence (gray box) or presence (black box) of GV-58 ($n = 8$). (E and F) Comparison of current amplitudes (E) and total charge flux (F) for cells expressing V-Ca $_v$ 2.1 R1624P in the absence (gray box) or presence (black box) of GV-58 ($n = 7$). Means and medians are indicated by the dashed and solid lines of the boxes, respectively. Boxes represent the 25th/75th percentiles. Bars represent the 5th/95th percentiles. Significant differences by two-tailed, paired t test are indicated.

consequential to a reduction of Ca^{2+} flux into the presynaptic nerve terminal. Swimming behavior and end-plate currents were both partially rescued by Roscovitine, a compound previously shown to stabilize the open state of wild-type Ca $_v$ 2.1 channels (Yan et al., 2002; Buraei et al., 2007). This latter observation prompted us to examine whether Ca^{2+} flux via Ca $_v$ 2.1 R1624P could be rescued to some degree with the higher-affinity Roscovitine derivative GV-58 (Tarr et al., 2013; Wu et al., 2018). In these experiments, GV-58 expectedly slowed deactivation of both the wild-type and mutant channels (Fig. 5). Interestingly, we also observed that GV-58 caused a 17-mV hyperpolarizing shift in channel activation of Ca $_v$ 2.1 R1624P, whereas there was only a 7-mV shift for wild-type Ca $_v$ 2.1. Given the position of the mutation in the S4 α -helix of repeat IV, this result suggests that GV-58 is facilitating movement of the RIV voltage sensor through the membrane field.

Ca^{2+} channel blockers are currently being employed to combat Ca $_v$ 2.1 R1673P pathology (Luo et al., 2017). Our data suggest that therapeutic agents that augment synaptic efficacy should be considered instead. One such compound, the carbonic anhydrase inhibitor acetazolamide, has been successful in blunting attacks of episodic ataxia 2 by increasing cycling of synaptic vesicles (Chen and Chesler, 1992; Bertone et al., 2017). However, the patient carrying the Ca $_v$ 2.1 R1673P mutation has been reported to be nonresponsive to this regimen (Luo et al., 2017). Since acetazolamide enhances synaptic efficacy at the level of vesicle cycling, it is possible that the lack of requisite Ca^{2+} flux into the terminal upstream from neurosecretion may have precluded its beneficial effects. In this regard, drugs that increase Ca $_v$ 2.1 P_o directly or prolong action potential duration may represent a better clinical regimen than drugs that target the vesicle release apparatus. While Roscovitine seems problematic because of the complexity of its effects on Ca $_v$ 2.1 and a variety of other ion channels (Yan et al., 2002; Buraei et al., 2005, 2007; Yarotsky and Elmslie, 2007, 2012), GV-58 is more consistent in its effects and may hold promise for further development (Tarr et al., 2013; Wu et al., 2018; S. Tyagi and R.A. Bannister, unpublished results). K^+ channel blockers have been approved to treat Lambert-Eaton myasthenic syndrome, an autoimmune condition in which Ca $_v$ 2.1 currents are depressed by autoantibodies directed to Ca $_v$ 2.1 (García and Beam, 1996). In particular, the promotion of synaptic efficacy through administration of 3,4-diaminopyridine, either alone or in combination with acetylcholinesterase inhibitors, has proven beneficial (Maddison, 2012).

Our results raise the possibility that an arginine to proline substitution at residue 1,673 causes a severe neurodevelopmental disorder by making Ca $_v$ 2.1 less sensitive to changes in membrane potential. However, it is important to point out that this conclusion is based on observations made with the rat orthologue. Another unfortunate limitation of our methodology is that we were unable to investigate the effects of the aforementioned compounds on motor behavior and synaptic function in the context of the mutation. Even though our heterologous expression system is an appropriate vehicle to assess the biophysical and pharmacological properties of the Ca $_v$ 2.1 R1673P mutant, there are multiple examples in which results obtained in neuronal cells have diverged from the outcomes predicted by work in heterologous systems. In particular, gain-of-function mutations in Ca $_v$ 2.1 and Na $_v$ 1.1 linked to familial hemiplegic migraine required a neuronal context to fully manifest as such (Tottene et al., 2002; Cestèle et al., 2013). The results of these latter studies underscore the need for a vertebrate model as an essential tool for understanding the fundamental biology of the syndrome associated with Ca $_v$ 2.1 R1673P and other cases of Ca $_v$ 2.1 loss-of-channel function, as well as the need to test the clinical suitability of 3,4-diaminopyridine, Roscovitine derivatives, and other (novel) compounds in combatting this growing family of severe neurological disorders.

Acknowledgments

We are grateful to Drs. P.J. Kammermeier (University of Rochester School of Medicine and Dentistry, Rochester, NY), B.A.

Adams (Utah State University, Logan, UT), and W.A. Sather (University of Colorado School of Medicine, Aurora, CO) for the gifts of the V-Ca_v2.1, β₄, and α₂δ-1 constructs, respectively. We thank Drs. K.G. Beam and A.B. Ribera for insightful discussion. Confocal images were acquired with the expert assistance of Dr. R. Moldovan of the CU Advanced Light Microscopy Core (National Center for Research Resources ULI RR025780).

This work was supported by National Institutes of Health grant NS103777 to R.A. Bannister and by a Boettcher Foundation Collaboration Grant to R.A. Bannister and S. Tyagi.

The authors declare no competing financial interests.

Author contributions: S. Tyagi, S. Papadopoulos, and R.A. Bannister designed research, performed research, analyzed data, and wrote the paper. T.R. Bendrick and D. Filipova performed research. All authors read and approved the final manuscript.

Sharona E. Gordon served as editor.

Submitted: 30 August 2018

Revised: 4 February 2019

Accepted: 18 March 2019

References

- Bahamonde, M.I., S.A. Serra, O. Drechsel, R. Rahman, A. Marcé-Grau, M. Prieto, S. Ossowski, A. Macaya, and J.M. Fernández-Fernández. 2015. A single amino acid deletion (ΔF1502) in the S6 segment of Ca_v2.1 domain III associated with congenital ataxia increases channel activity and promotes Ca²⁺ influx. *PLoS One*. 10:e0146035. <https://doi.org/10.1371/journal.pone.0146035>
- Beqollari, D., and P.J. Kammermeier. 2013. The interaction between mGluR1 and the calcium channel Cav_{2.1} preserves coupling in the presence of long Homer proteins. *Neuropharmacology*. 66:302–310. <https://doi.org/10.1016/j.neuropharm.2012.05.038>
- Beqollari, D., C.F. Romberg, D. Filipova, S. Papadopoulos, and R.A. Bannister. 2015. Functional assessment of three Rem residues identified as critical for interactions with Ca(2+) channel β subunits. *Pflugers Arch*. 467: 2299–2306. <https://doi.org/10.1007/s00424-015-1700-x>
- Beqollari, D., K. Dockstader, and R.A. Bannister. 2018. A skeletal muscle L-type Ca²⁺ channel with a mutation in the selectivity filter (Ca_v1.1 E1014K) conducts K<sup>[>]. *J. Biol. Chem*. 293:3126–3133. <https://doi.org/10.1074/jbc.M117.812446>
- Bertone, N.I., A.I. Groisman, G.L. Mazzone, R. Cano, L. Tabares, and O.D. Uchitel. 2017. Carbonic anhydrase inhibitor acetazolamide shifts synaptic vesicle recycling to a fast mode at the mouse neuromuscular junction. *Synapse*. 71:12. <https://doi.org/10.1002/syn.22009>
- Blumkin, L., M. Michelson, E. Leshinsky-Silver, S. Kivity, D. Lev, and T. Lerman-Sagie. 2010. Congenital ataxia, mental retardation, and dyskinesia associated with a novel CACNA1A mutation. *J. Child Neurol*. 25: 892–897. <https://doi.org/10.1177/0883073809351316>
- Buraei, Z., M. Anghelescu, and K.S. Elmslie. 2005. Slowed N-type calcium channel (Ca_v2.2) deactivation by the cyclin-dependent kinase inhibitor roscovitine. *Biophys. J*. 89:1681–1691. <https://doi.org/10.1529/biophysj.104.052837>
- Buraei, Z., G. Schofield, and K.S. Elmslie. 2007. Roscovitine differentially affects Ca_v2 and K_v channels by binding to the open state. *Neuropharmacology*. 52:883–894. <https://doi.org/10.1016/j.neuropharm.2006.10.006>
- Campiglio, M., and B.E. Flucher. 2015. The role of auxiliary subunits for the functional diversity of voltage-gated calcium channels. *J. Cell. Physiol*. 230:2019–2031. <https://doi.org/10.1002/jcp.24998>
- Cao, Y.Q., and R.W. Tsien. 2010. Different relationship of N- and P/Q-type Ca²⁺ channels to channel-interacting slots in controlling neurotransmission at cultured hippocampal synapses. *J. Neurosci*. 30: 4536–4546. <https://doi.org/10.1523/JNEUROSCI.5161-09.2010>
- Cao, Y.Q., E.S. Piedras-Rentería, G.B. Smith, G. Chen, N.C. Harata, and R.W. Tsien. 2004. Presynaptic Ca²⁺ channels compete for channel type-preferring slots in altered neurotransmission arising from Ca²⁺ channelopathy. *Neuron*. 43:387–400. <https://doi.org/10.1016/j.neuron.2004.07.014>
- Cestèle, S., E. Schiavon, R. Rusconi, S. Franceschetti, and M. Mantegazza. 2013. Nonfunctional Nav1.1 familial hemiplegic migraine mutant transformed into gain of function by partial rescue of folding defects. *Proc. Natl. Acad. Sci. USA*. 110:17546–17551. <https://doi.org/10.1073/pnas.1309827110>
- Chen, J.C., and M. Chesler. 1992. pH transients evoked by excitatory synaptic transmission are increased by inhibition of extracellular carbonic anhydrase. *Proc. Natl. Acad. Sci. USA*. 89:7786–7790. <https://doi.org/10.1073/pnas.89.16.7786>
- Dunlap, K., J.I. Luebke, and T.J. Turner. 1994. Identification of calcium channels that control neurosecretion. *Science*. 266:828–831. <https://doi.org/10.1126/science.7973643>
- Dunlap, K., J.I. Luebke, and T.J. Turner. 1995. Exocytotic Ca²⁺ channels in mammalian central neurons. *Trends Neurosci*. 18:89–98. [https://doi.org/10.1016/0166-2236\(95\)80030-6](https://doi.org/10.1016/0166-2236(95)80030-6)
- Fujita, Y., M. Mynlieff, R.T. Dirksen, M.-S. Kim, T. Niidome, J. Nakai, T. Friedrich, N. Iwabe, T. Miyata, T. Furuichi, et al 1993. Primary structure and functional expression of the ω-conotoxin-sensitive N-type calcium channel from rabbit brain. *Neuron*. 10:585–598. [https://doi.org/10.1016/0896-6273\(93\)90162-K](https://doi.org/10.1016/0896-6273(93)90162-K)
- García, K.D., and K.G. Beam. 1996. Reduction of calcium currents by Lambert-Eaton syndrome sera: motoneurons are preferentially affected, and L-type currents are spared. *J. Neurosci*. 16:4903–4913. <https://doi.org/10.1523/JNEUROSCI.16-16-04903.1996>
- Grabner, M., R.T. Dirksen, and K.G. Beam. 1998. Tagging with green fluorescent protein reveals a distinct subcellular distribution of L-type and non-L-type Ca²⁺ channels expressed in dysgenic myotubes. *Proc. Natl. Acad. Sci. USA*. 95:1903–1908. <https://doi.org/10.1073/pnas.95.4.1903>
- Hamill, O.P., A. Marty, E. Neher, B. Sakmann, and F.J. Sigworth. 1981. Improved patch-clamp techniques for high-resolution current recording from cells and cell-free membrane patches. *Pflugers Arch*. 391:85–100. <https://doi.org/10.1007/BF00656997>
- Hans, M., S. Luvisetto, M.E. Williams, M. Spagnolo, A. Urrutia, A. Tottene, P.F. Brust, E.C. Johnson, M.M. Harpold, K.A. Stauderman, and D. Pié-trobon. 1999. Functional consequences of mutations in the human α_{1A} calcium channel subunit linked to familial hemiplegic migraine. *J. Neurosci*. 19:1610–1619. <https://doi.org/10.1523/JNEUROSCI.19-05-01610.1999>
- Jen, J., J. Wan, M. Graves, H. Yu, A.F. Mock, C.J. Coulin, G. Kim, Q. Yue, D.M. Papazian, and R.W. Baloh. 2001. Loss-of-function EA2 mutations are associated with impaired neuromuscular transmission. *Neurology*. 57: 1843–1848. <https://doi.org/10.1212/WNL.57.10.1843>
- Kaja, S., R.C. Van De Ven, R.R. Frants, M.D. Ferrari, A.M. Van Den Maagdenberg, and J.J. Plomp. 2008. Reduced ACh release at neuromuscular synapses of heterozygous leaner Ca_v2.1-mutant mice. *Synapse*. 62: 337–344. <https://doi.org/10.1002/syn.20490>
- Katz, B., and R. Miledi. 1967. A study of synaptic transmission in the absence of nerve impulses. *J. Physiol*. 192:407–436. <https://doi.org/10.1113/jphysiol.1967.sp008307>
- Llinás, R., I.Z. Steinberg, and K. Walton. 1981. Presynaptic calcium currents in squid giant synapse. *Biophys. J*. 33:289–321. [https://doi.org/10.1016/S0006-3495\(81\)84898-9](https://doi.org/10.1016/S0006-3495(81)84898-9)
- Lübbert, M., R.O. Goral, C. Keine, C. Thomas, D. Guerrero-Given, T. Putzke, R. Satterfield, N. Kamasawa, and S.M. Young Jr. 2019. Ca_v2.1 α₁ subunit expression regulates presynaptic Ca_v2.1 abundance and synaptic strength at a central synapse. *Neuron*. 101:260–273. <https://doi.org/10.1016/j.neuron.2018.11.028>
- Luo, X., J.A. Rosenfeld, S. Yamamoto, T. Harel, Z. Zuo, M. Hall, K.J. Wierenga, M.T. Pastore, D. Bartholomew, M.R. Delgado, et al; Members of the UDN. 2017. Clinically severe CACNA1A alleles affect synaptic function and neurodegeneration differentially. *PLoS Genet*. 13:e1006905. <https://doi.org/10.1371/journal.pgen.1006905>
- Lv, Y., Z. Wang, C. Liu, and L. Cui. 2017. Identification of a novel CACNA1A mutation in a Chinese family with autosomal recessive progressive myoclonic epilepsy. *Neuropsychiatr. Dis. Treat*. 13:2631–2636. <https://doi.org/10.2147/NDT.S145774>
- Maddison, P. 2012. Treatment in Lambert-Eaton myasthenic syndrome. *Ann. N. Y. Acad. Sci*. 1275:78–84. <https://doi.org/10.1111/j.1749-6632.2012.06769.x>
- Maselli, R.A., J. Wan, V. Dunne, M. Graves, R.W. Baloh, R.L. Wollmann, and J. Jen. 2003. Presynaptic failure of neuromuscular transmission and synaptic remodeling in EA2. *Neurology*. 61:1743–1748. <https://doi.org/10.1212/01.WNL.0000099748.41130.9A>
- Meza, U., and B. Adams. 1998. G-Protein-dependent facilitation of neuronal α_{1A}, α_{1B}, and α_{1E} Ca channels. *J. Neurosci*. 18:5240–5252. <https://doi.org/10.1523/JNEUROSCI.18-14-05240.1998>

- Molina-Campos, E., Y. Xu, and W.D. Atchison. 2015. Age-dependent contribution of P/Q- and R-type Ca^{2+} channels to neuromuscular transmission in *lethargic* mice. *J. Pharmacol. Exp. Ther.* 352:395–404. <https://doi.org/10.1124/jpet.114.216143>
- Mori, Y., T. Friedrich, M.S. Kim, A. Mikami, J. Nakai, P. Ruth, E. Bosse, F. Hofmann, V. Flockerzi, T. Furuichi, et al 1991. Primary structure and functional expression from complementary DNA of a brain calcium channel. *Nature.* 350:398–402. <https://doi.org/10.1038/350398a0>
- Mori, Y., M. Wakamori, S. Oda, C.F. Fletcher, N. Sekiguchi, E. Mori, N.G. Copeland, N.A. Jenkins, K. Matsushita, Z. Matsuyama, and K. Imoto. 2000. Reduced voltage sensitivity of activation of P/Q-type Ca^{2+} channels is associated with the ataxic mouse mutation rolling Nagoya (*tg(rol)*). *J. Neurosci.* 20:5654–5662. <https://doi.org/10.1523/JNEUROSCI.20-15-05654.2000>
- Pagani, R., M. Song, M. McEnery, N. Qin, R.W. Tsien, L. Toro, E. Stefani, and O.D. Uchitel. 2004. Differential expression of α_1 and β subunits of voltage dependent Ca^{2+} channel at the neuromuscular junction of normal and P/Q Ca^{2+} channel knockout mouse. *Neuroscience.* 123:75–85. <https://doi.org/10.1016/j.neuroscience.2003.09.019>
- Palovcak, E., L. Delemotte, M.L. Klein, and V. Carnevale. 2014. Evolutionary imprint of activation: the design principles of VSDs. *J. Gen. Physiol.* 143: 145–156. <https://doi.org/10.1085/jgp.201311103>
- Piétrobon, D. 2010. $\text{Ca}_v2.1$ channelopathies. *Pflügers Archiv-Eur. J. Physiol.* 460: 375–393.
- Romaniello, R., C. Zucca, A. Tonelli, S. Bonato, C. Baschiroto, N. Zanotta, R. Epifanio, A. Righini, N. Bresolin, M.T. Bassi, and R. Borgatti. 2010. A wide spectrum of clinical, neurophysiological and neuroradiological abnormalities in a family with a novel CACNA1A mutation. *J. Neurol. Neurosurg. Psychiatry.* 81:840–843. <https://doi.org/10.1136/jnnp.2008.163402>
- Splawski, I., K.W. Timothy, L.M. Sharpe, N. Decher, P. Kumar, R. Bloise, C. Napolitano, P.J. Schwartz, R.M. Joseph, K. Condouris, et al 2004. $\text{Ca}_v1.2$ calcium channel dysfunction causes a multisystem disorder including arrhythmia and autism. *Cell.* 119:19–31. <https://doi.org/10.1016/j.cell.2004.09.011>
- Splawski, I., K.W. Timothy, N. Decher, P. Kumar, F.B. Sachse, A.H. Beggs, M.C. Sanguinetti, and M.T. Keating. 2005. Severe arrhythmia disorder caused by cardiac L-type calcium channel mutations. *Proc. Natl. Acad. Sci. USA.* 102:8089–8096, discussion :8086–8088. <https://doi.org/10.1073/pnas.0502506102>
- Stühmer, W., F. Conti, H. Suzuki, X.D. Wang, M. Noda, N. Yahagi, H. Kubo, and S. Numa. 1989. Structural parts involved in activation and inactivation of the sodium channel. *Nature.* 339:597–603. <https://doi.org/10.1038/339597a0>
- Tao, X., A. Lee, W. Limapichat, D.A. Dougherty, and R. MacKinnon. 2010. A gating charge transfer center in voltage sensors. *Science.* 328:67–73. <https://doi.org/10.1126/science.1185954>
- Tarr, T.B., W. Malick, M. Liang, G. Valdomir, M. Frasso, D. Lacomis, S.W. Reddel, A. Garcia-Ocano, P. Wipf, and S.D. Meriney. 2013. Evaluation of a novel calcium channel agonist for therapeutic potential in Lambert-Eaton myasthenic syndrome. *J. Neurosci.* 33:10559–10567. <https://doi.org/10.1523/JNEUROSCI.4629-12.2013>
- Tottene, A., T. Fellin, S. Pagnutti, S. Luvisetto, J. Striessnig, C. Fletcher, and D. Piétrobon. 2002. Familial hemiplegic migraine mutations increase Ca^{2+} influx through single human $\text{Ca}_v2.1$ channels and decrease maximal $\text{Ca}_v2.1$ current density in neurons. *Proc. Natl. Acad. Sci. USA.* 99: 13284–13289. <https://doi.org/10.1073/pnas.192242399>
- Travaglini, L., M. Nardella, E. Bellacchio, A. D'Amico, A. Capuano, R. Fruscante, M. Di Capua, R. Cusmai, S. Barresi, S. Morlino, et al 2017. Missense mutations of CACNA1A are a frequent cause of autosomal dominant nonprogressive congenital ataxia. *Eur. J. Paediatr. Neurol.* 21: 450–456. <https://doi.org/10.1016/j.ejpn.2016.11.005>
- Turner, T.J., M.E. Adams, and K. Dunlap. 1992. Calcium channels coupled to glutamate release identified by ω -Aga-IVA. *Science.* 258:310–313. <https://doi.org/10.1126/science.1357749>
- Uchitel, O.D., D.A. Protti, V. Sanchez, B.D. Cherksey, M. Sugimori, and R. Llinás. 1992. P-type voltage-dependent calcium channel mediates presynaptic calcium influx and transmitter release in mammalian synapses. *Proc. Natl. Acad. Sci. USA.* 89:3330–3333. <https://doi.org/10.1073/pnas.89.8.3330>
- Volsen, S.G., N.C. Day, A.L. McCormack, W. Smith, P.J. Craig, R.E. Beattie, D. Smith, P.G. Ince, P.J. Shaw, S.B. Ellis, et al 1997. The expression of voltage-dependent calcium channel beta subunits in human cerebellum. *Neuroscience.* 80:161–174. [https://doi.org/10.1016/S0306-4522\(97\)00115-2](https://doi.org/10.1016/S0306-4522(97)00115-2)
- Wappl, E., A. Koschak, M. Poteser, M.J. Sinnegger, D. Walter, A. Eberhart, K. Groschner, H. Glossmann, R.L. Kraus, M. Grabner, and J. Striessnig. 2002. Functional consequences of P/Q-type Ca^{2+} channel $\text{Ca}_v2.1$ missense mutations associated with episodic ataxia type 2 and progressive ataxia. *J. Biol. Chem.* 277:6960–6966. <https://doi.org/10.1074/jbc.M110948200>
- Wen, H., M.W. Linhoff, J.M. Hubbard, N.R. Nelson, D. Stensland, J. Dallman, G. Mandel, and P. Brehm. 2013. Zebrafish calls for reinterpretation for the roles of P/Q calcium channels in neuromuscular transmission. *J. Neurosci.* 33:7384–7392. <https://doi.org/10.1523/JNEUROSCI.5839-12.2013>
- Weyhrauch, D.L., D. Ye, N.J. Boczek, D.J. Tester, R.H. Gavrilo, M.C. Patterson, E.D. Wieben, and M.J. Ackerman. 2016. Whole exome sequencing and heterologous cellular electrophysiology studies elucidate a novel loss-of-function mutation in the CACNA1A-encoded neuronal P/Q-type calcium channel in a child with congenital hypotonia and developmental delay. *Pediatr. Neurol.* 55:46–51. <https://doi.org/10.1016/j.pediatrneurol.2015.10.014>
- Wu, L.-G., and P. Saggau. 1997. Presynaptic inhibition of elicited neurotransmitter release. *Trends Neurosci.* 20:204–212. [https://doi.org/10.1016/S0166-2236\(96\)01015-6](https://doi.org/10.1016/S0166-2236(96)01015-6)
- Wu, M., H.V. White, B.A. Boehm, C.J. Meriney, K. Kerrigan, M. Frasso, M. Liang, E.M. Gotway, M.R. Wilcox, J.W. Johnson, et al 2018. New Ca_v2 calcium channel gating modifiers with agonist activity and therapeutic potential to treat neuromuscular disease. *Neuropharmacology.* 131: 176–189. <https://doi.org/10.1016/j.neuropharm.2017.12.022>
- Yan, Z., P. Chi, J.A. Bibb, T.A. Ryan, and P. Greengard. 2002. Roscovitine: a novel regulator of P/Q-type calcium channels and transmitter release in central neurons. *J. Physiol.* 540:761–770. <https://doi.org/10.1113/jphysiol.2001.013376>
- Yarotsky, V., and K.S. Elmslie. 2007. Roscovitine, a cyclin-dependent kinase inhibitor, affects several gating mechanisms to inhibit cardiac L-type ($\text{Ca}_v1.2$) calcium channels. *Br. J. Pharmacol.* 152:386–395. <https://doi.org/10.1038/sj.bjp.0707414>
- Yarotsky, V., and K.S. Elmslie. 2012. Roscovitine inhibits $\text{Ca}_v3.1$ (T-type) channels by preferentially affecting closed-state inactivation. *J. Pharmacol. Exp. Ther.* 340:463–472. <https://doi.org/10.1124/jpet.111.187104>